Article

Effects of 222 nm Germicidal Ultraviolet Light on Aerosol and VOC Formation from Limonene

Olivia J. Jenks, Zhe Peng, Melinda K. Schueneman, Madison Rutherford, Anne V. Handschy, Douglas A. Day, Jose L. Jimenez, and Joost A. de Gouw*

Read Online

ACCESS	Metrics & More	Article Recommendations	Supporting Information

ABSTRACT: Since the 1930s, germicidal ultraviolet (GUV) irradiation has been used indoors to prevent the transmission of airborne diseases, such as tuberculosis and measles. Recently, it has received renewed attention due to the COVID-19 pandemic. While GUV radiation has been shown to be effective in inactivating airborne bacteria and viruses, few studies on the impact of GUV on indoor air quality have been published. In this work, we evaluate the effects of GUV222 (GUV at 222 nm) on the chemistry of a common indoor volatile organic compound (VOC), limonene. We found that the production of O_3 by the GUV222 lamps caused the formation of particulate matter (PM) and oxygenated volatile organic compounds (VOCs). We also found that the chemistry proceeds through the ozonolysis of limonene as well as the reaction with secondary OH, and that the presence of GUV light led to observable but small perturbations to this chemistry. Understanding the effects of GUV222 on indoor air quality is important in evaluating the safety of these devices.

KEYWORDS: atmospheric chemistry, monoterpene, indoor air quality, UVGI, disinfection, particulate matter
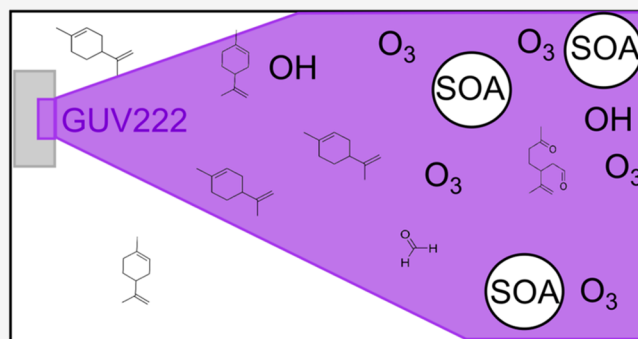
INTRODUCTION

Since the mid-1800s it has been known that light affects microorganisms, and germicidal ultraviolet (GUV), also known as ultraviolet germicidal irradiation (UVGI) has been used to inactivate airborne microbes since the early 1900s.[1] GUV light fixtures have been installed in hospitals to decrease postoperative wound infections and prevent the spread of tuberculosis and influenza, as well as in schools to prevent the transmission of measles.[2−5] The use of GUV decreased in the mid-1900s partially due to the development of antibiotics and immunizations, and also due to the perceived low importance of airborne transmission.[1,6] Recently, there has been renewed interest in GUV for air disinfection because of the COVID-19 pandemic, for which airborne transmission was found to be important.[6,7] Studies have shown that UV lamps at 254 nm (GUV254) and 222 nm (GUV222) are effective in inactivating SARS-CoV-2.[8,9]

One limitation of using 254 nm UV (GUV254) fixtures for air disinfection is that they are not safe for human exposure, so they are usually either mounted near the ceiling for upper room irradiation or used inside ventilation ducts.[10,11] Studies have shown that 222 nm lamps can be used for whole-room disinfection to inactivate airborne bacteria and viruses without harm to human skin and eyes.[12−14] However, it has also been shown that GUV222 forms substantial ozone, which can react

further in the indoor environment to form harmful pollutants like formaldehyde and $PM_{2.5}$.[15−17]

Given that the majority of people in the developed world spend a large fraction of their time indoors, ensuring good indoor air quality is crucial for promoting overall health and well-being.[18] Volatile organic compounds (VOCs) can be emitted from many sources indoors including cleaning products, paint, furniture, and humans.[19,20] Some of these VOCs, like formaldehyde are known to have negative health effects.[21,22] Some compounds undergo reactions to produce hazardous products, such as secondary organic aerosol (SOA). For example, a study by Graeffe et al. (2023) showed that commercial GUV254 devices can increase particle number concentrations and gas-phase species concentrations in indoor air.[23]

This work evaluates the effects of GUV222 on the chemistry of limonene and its oxidation products. Limonene, a common fragrance ingredient in personal care and cleaning products, is one of the most common VOCs in indoor air.[20,24] Limonene is

also highly reactive with hydroxyl (OH), ozone (O_3) and nitrate (NO_3). Ozone, a common indoor pollutant, comes from outdoor air, can be enhanced by GUV222 and reacts with VOCs like limonene.[25] Limonene ozonolysis can be a significant source of particulate matter (PM) indoors and can also form gas-phase products such as formaldehyde and glyoxal.[26−29] While limonene ozonolysis has been studied in detail, the question we focus on here is whether the formation of products is modified by the presence of GUV222. For example, photolysis could potentially remove species with carbonyl and acid groups as observed by Deal and Vaida (2023) for lactic acid.[30]

In this paper, we study the chemistry of limonene induced by GUV222 in an environmental chamber. We address how well a commonly used chemical mechanism, the Regional Atmospheric Chemistry Mechanism (RACM), with modifications that account for SOA formation and wall loss in a chamber, predicts limonene removal and SOA formation under the experimental conditions used in the chamber.[31] We then analyze in detail whether the 222 nm light impacts the formation of gas-phase and particle-phase oxidation products. This work builds on previous studies that focused on the formation of O_3 by GUV222 and the modeling of that formation.[15,32]

■ MATERIALS AND METHODS

Chamber Experiments. Chamber experiments were conducted in an ∼21 m^3 Teflon FEP chamber. Clean air was supplied to the chamber with AADCO 737-15A clean air generators (NO_x <0.2 ppb; VOC <50 ppb). One Ushio B1 KrCl excimer 222 nm lamp with an average fluence rate of 2.3 μW cm^{-2} (about 1/3 of the eye limit set by the American Conference of Governmental Industrial Hygienists, ACGIH) was placed inside the chamber, which has previously been shown to lead to rapid ozone formation.[15,33] The emission spectrum is shown in Figure S1. Here, ∼20 ppb ozone (average concentrations across many indoor spaces without GUV are between 4 and 6 ppb, and range between 1 and 31 ppb) was produced in two steps of 30 min with 15 min in between.[34] Liquid precursor (limonene or hexanal) was then evaporated into the chamber using a glass bulb under nitrogen flow to produce a ∼20 ppb concentration (typical indoor spaces have concentrations of limonene between 4 and 12 ppb).[35,36] An experiment using α-pinene as the precursor was also performed for comparison to the results of the limonene experiments. However, these results are not analyzed in further detail. The results for this experiment are shown in Figure S2. A Teflon-coated fan was run during these additions for about 2 min to ensure complete mixing in the chamber. The 222 nm lamp was turned on continuously for several hours or alternated in steps of 30 min on/off. Experiments were performed at ambient pressure (∼830 mbar in Boulder, CO), room temperature (25-27 °C), and low (<1%) and moderate (∼25%) RH. Experiment summaries are shown in Table S1 and Figure 1. Further details on the environmental chamber facility have been described in several previous publications.[15,37−39]

Chemicals. The following chemicals with purities and suppliers were used: (R)-(+)-limonene (97%) and hexanal (99%) from Aldrich Chemical Company; acetone (99%) from Sigma-Aldrich; ultrahigh purity (UHP) N_2 from Airgas; and a standard gas mixture (methanol, acetonitrile, acetaldehyde, acetone, acrylonitrile, isoprene, 2-butanone, benzene, toluene, m-xylene, 1,2,4-trimethylbenzene, α-pinene, and β-caryophyl-
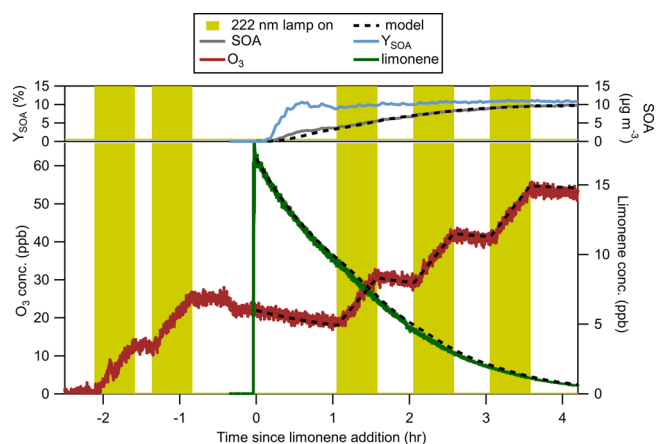

Figure 1. Modeled and experimental time series of limonene, ozone, SOA mass concentration, and SOA mass yield for an experiment under dry conditions.

lene in N_2) from Apel-Riemer to calibrate the Vocus proton-transfer-reaction time-of-flight mass spectrometer (see Instrumentation).

Instrumentation. A Tofwerk AG and Aerodyne Research Inc. Vocus 2R proton-transfer-reaction time-of-flight mass spectrometer (PTR-TOF) was used to measure VOCs, including limonene and its gas-phase ozonolysis products. A 2-m long Teflon sample line was used with a flow rate of ∼2 LPM (0.635 cm OD, 0.397 cm ID). The FIMR DC voltage was 500 V, the RF voltage amplitude was 400 V at 1.3 MHz, and the FIMR pressure was 1.5 mbar, resulting in an E/N of ∼160 Td. PTR-TOF data were obtained at 1 Hz. The PTR-TOF was calibrated using a standard gas mixture containing several VOCs (see above). For VOCs not contained in this mixture such as limonene, we used calculated sensitivities based on the quantitative liquid amount injected into the known chamber volume.

Ozone was monitored by using a Thermo Scientific 49i Ozone Analyzer. The SOA concentration was obtained primarily through scanning mobility particle sizer measurements (SMPS, TSI models: 3080 electrostatic classifier, 3081 differential mobility analyzer, and 3775 condensation particle counter). In one instance, a high-resolution time-of-flight aerosol mass spectrometer (AMS, Aerodyne Research, Inc., described in DeCarlo et al., 2006) was used to obtain chemical composition measurements.[40] The size distributions using the SMPS were measured every 135 s, and the volume distributions were integrated over a 16-600 nm mobility diameter range. The AMS was run in the "fast mass spec" mode (FMS), where data was obtained at 1 Hz.[41,42] The average resolution ($m/\Delta m$) at m/z < 120 was ∼2500. Copper and/or stainless-steel tubing was used for the aerosol measurements with a sample flow rate of ∼1 LPM (0.635 cm OD, 0.380 cm ID, ∼1.2 m long for AMS, ∼2.5 m for SMPS).

Data Processing. Tofware (v3.2.3, www.tofwerk.com/tofware) in the Igor Pro 8 (Wavemetrics, OR, USA) environment was used for processing the PTR-TOF data. Peaks were assigned elemental formulas manually, and the time series of these peak integrals were calculated using the peak shape fit. Mass-to-charge ratio calibration was performed using a few selected ions between m/z 45 and 297. Backgrounds were measured from the clean chamber immediately before the

addition of the precursor. In the hexanal experiments, the decrease in hexanal was very slow, and care must be taken to differentiate the chemical loss of hexanal versus a drift in detection sensitivity. For this purpose, acetone was used as a tracer of PTR-TOF sensitivity throughout the dry and humid hexanal experiments. In those experiments, PTR-TOF data were normalized to 2×10^5 cps of $C_3H_6OH^+$, which is indicated by the units of normalized counts per second (ncps). For the limonene experiments, the PTR-TOF data were not normalized.

AMS data were processed using Squirrel (version 1.65F) and PIKA (version 1.25F) in the Igor Pro 8 (Wavemetrics, OR, USA) environment.[43] The SMPS measures size particle number distributions and these were converted to integrated volume concentrations using custom software in the Igor Pro 8 environment.[44] The volume concentrations were converted to mass concentrations by multiplying the SMPS volume concentration by the density derived from AMS elemental ratios (O:C, H:C), as described in Kuwata et al., (2012) and shown in Figure S3.[45] The O:C and H:C ratios were calculated as described in Canagaratna et. al. (2015).[46] The AMS SOA concentration was corrected for differences from the default AMS OA relative ionization efficiency (RIE, 1.4) and collection efficiency (CE, 1) (RIE*CE of 1.4) by calibrating the AMS to the measured SMPS SOA mass concentration (using a single factor determined from a linear regression).[47,48] This was necessary since organic RIE and CE can vary by as much as factors of 2-3 for chamber-generated SOA and standards.[33,42,43] The condensational sink (CS) was calculated from particle size distribution measured by the SMPS per eq 1.[49]

$$CS = 2\pi D \sum_i \beta_i d_i N_i \tag{1}$$

where d_i, N_i, and β_i are the diameter, the number concentration, and the Fuchs–Sutugin correction factor of the particles in the ith size bin, respectively, and D is the diffusion coefficient of the condensable organic gases (assumed to be 7×10^{-6} m^2 s^{-1}). The calculated CS is shown in Figure S4.

Kinetic Modeling. A kinetic model for the limonene ozonolysis chamber experiments was built and run in KinSim version 4.24 (a kinetics simulator developed for educational and research purposes) within Igor Pro 8.[50] This model was based on the model in Peng et al. (2023) with the mechanisms for gas-phase inorganic and organic chemistries being the oxidation flow reactor chemical mechanism and part of the RACM, respectively.[31,32,51] The reactions relevant to the formation of SOA from limonene (Table S2) are not part of this gas-phase chemistry but are parallel to it. The gas-phase and SOA-related chemistries do not affect each other except through limonene, OH, and O_3 concentrations. The SOA formation mechanism was built separately for this model as the RACM does not have good skill in simulating SOA formation. The condensable product formation, the gas-particle partitioning, the wall losses of gas- and particle-phase products in the model were simulated in a dynamical manner based on Krechmer et al. (2020), but with different values for several key parameters.[52] The condensation sink for modeling was constrained by SMPS measurements (Figure S4). The SMPS could not sufficiently detect the ultrafine particles <16 nm (the DMA scanning range) that were formed in a large number during that period. To avoid possible biases, that period was thus excluded for the fitting that estimated the molar yields of

condensable products. In the model, the first-generation oxidation of limonene is assumed to produce two products, a semivolatile species (SVOC) and a low-volatility species (LVOC), with saturation mass concentrations of 10 and 0.0001 μg m^{-3}, respectively, and molecular weights of 250 g mol^{-1}. The second-generation oxidation is assumed to only convert SVOC to LVOC. The molar yields of the first-generation SVOC and LVOC and the second-generation LVOC were determined by a fitting that varied them to minimize the sum of the squared deviations of the modeled SOA concentrations at different times from the corresponding measurements. Both OH and O_3 can be the oxidant of these oxidation reactions, with rate coefficients reported in Table S2. The lifetime for condensable gases to deposit onto chamber walls in the model was 1000 s.[52] The evaporation rates of gases partitioned to chamber walls were calculated per Liu et al. (2019).[37] To best fit the experimental results, the particle deposition rate in the chamber was fitted as 0.052 h^{-1}, which is consistent with other experiments conducted in this chamber.[37,38] The deposition rate for OH is insignificant due to its short lifetime and the dry deposition of ozone is very slow, as documented in Peng et al. (2023).[15]
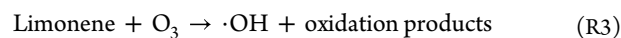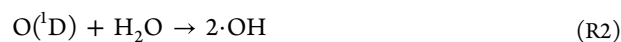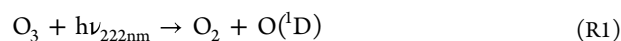
■ RESULTS AND DISCUSSION

Gas-Phase Removal of Limonene. Results of limonene chamber experiments under dry conditions are shown in Figure 1 and those under humid conditions in Figure S5. Prior to the addition of limonene to the chamber, O_3 was produced by the 222 nm lamp in 2 steps. The O_3 production rate during these steps was measured at ~24 ppb hr^{-1}, which is consistent with previous measurements.[15] At time zero, limonene was added to the chamber. Ozonolysis of limonene leads to removal of limonene and O_3, and to formation of SOA. After 1 h, the GUV222 lamp was switched on and then alternated on a 30 min on−off cycle. When the GUV222 lamp was on, the O_3 started to increase again, and as will be shown below, the removal of limonene and the formation of SOA were accelerated at these times. Also included in Figure 1 are the model results for the concentrations of limonene, O_3, and SOA.

In Figure 2A, the limonene data from Figure 1 are again shown. While the data appear to show an approximate exponential loss, this should not be the case, since O_3 was not constant. The limonene loss rate, -d[LIM]/dt (Figure 2B), is described by

$$\frac{d[\text{lim}]}{dt} = -k_{\text{lim}+O_3}[\text{lim}][O_3] - k_{\text{lim}+OH}[\text{lim}][OH] \tag{2}$$

in which the concentrations of limonene, [LIM], ozone, [O_3], and hydroxyl, [OH], all vary in time. We include hydroxyl (OH) reactions here for 2 reasons: (i) primary OH can be formed from ozone photolysis (Reaction R1 and Reaction R2), and (ii) secondary OH can be formed from limonene ozonolysis (Reaction R3).

$$O_3 + h\nu_{222nm} \rightarrow O_2 + O(^1D) \tag{R1}$$

$$O(^1D) + H_2O \rightarrow 2\cdot OH \tag{R2}$$

$$\text{Limonene} + O_3 \rightarrow \cdot OH + \text{oxidation products} \tag{R3}$$

It is seen from Figure 2B that the limonene loss rate shows a clear kink when the GUV222 lamp comes on at t=1 h. At this time, the level of O_3 starts to increase again due to the
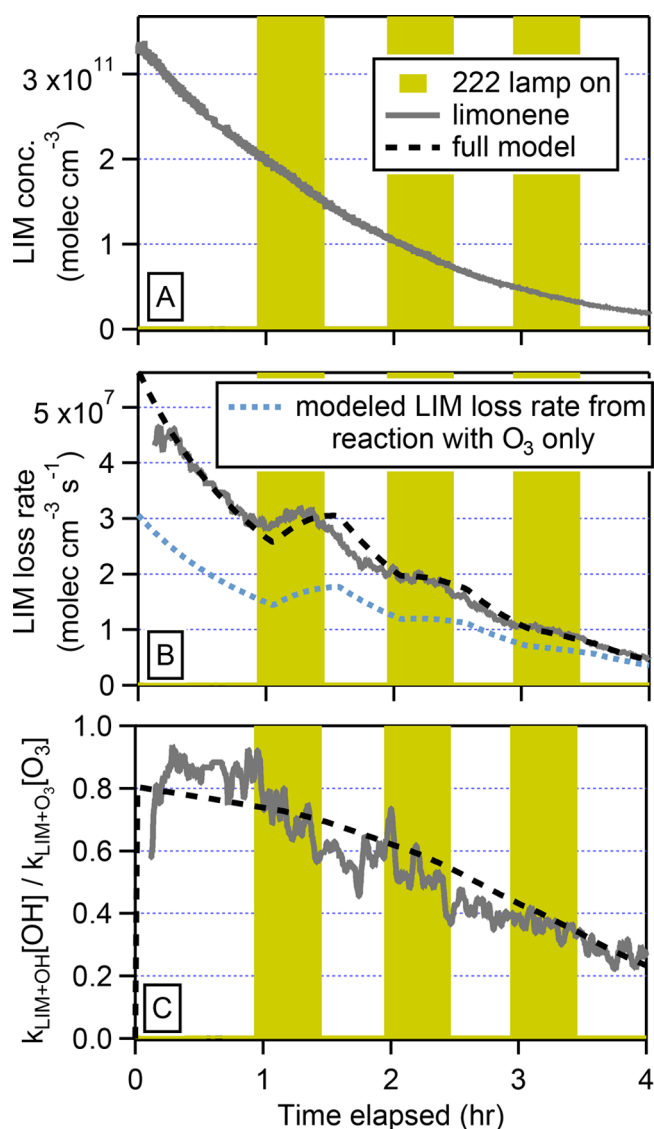
Figure 2. Time series of limonene (LIM) reacting with O_3 measured by the PTR-TOF under dry conditions, similar to Figure 1, but now in units of molecules cm^{-3} (A); the modeled and experimental loss rate of limonene and the modeled loss rate of limonene due to only O_3 (B) per eq 2); and modeled and experimental $k_{LIM+OH}[OH]$ / $k_{LIM+O3}[O_3]$ (C) per eq 3.

GUV222 lamp and the limonene loss rate increases. Similar changes in slope in the limonene loss rate can also be seen at t=2 h and t=3 h, though less clearly. Also added to Figure 2B is the limonene loss rate that can be explained from ozone only (first term on the right-hand side of eq 2. The ozone reaction does not fully account for the observed loss rate of limonene, and the difference can be explained by OH as will be shown quantitatively below. We conclude that the decrease in limonene is not a simple exponential in time but that it is modulated by the GUV222 light, which enhances the concentrations of O_3 and OH in the chamber.

To address the loss of limonene by OH, we can rearrange eq 2 as follows:

$$\frac{k_{\text{lim}+OH}[OH]}{k_{\text{lim}+O_3}[O_3]} = -\frac{\frac{d[\text{lim}]}{dt}}{k_{\text{lim}+O_3}[\text{lim}][O_3]} - 1 \qquad (3)$$

The term on the left represents the relative loss rates of limonene in the reaction with OH and O_3, respectively. The term on the right is composed of measured concentrations and the literature values for the bimolecular rate coefficient for the reaction of ozone with limonene (k_{LIM+O3} = 2.0× 10^{-16} cm^3 molecules^{-1} s^{-1}) and the bimolecular rate coefficient for the reaction of OH with limonene (k_{LIM+OH} = 1.7× 10^{-10} cm^3 molecules^{-1} s^{-1}).[53,54] Figure 2C shows the numerical value for the parameter $k_{LIM+OH}[OH]$ / $k_{LIM+O3}[O_3]$ calculated from the data using Equation 3. The ratio is initially around 1, indicating that limonene is removed by OH and O_3 at equal rates. Later, the ratio approaches zero and limonene is consumed. As a result, the secondary formation of OH slows and the OH that is generated can also react with limonene oxidation products. Also shown in Figure 2C is the parameter $k_{LIM+OH}[OH]$ / $k_{LIM+O3}[O_3]$ calculated from the model. The excellent agreement with the data shows that the removal of limonene by O_3 and OH, as well as the formation of OH, is well represented in the mechanism. The time series also gives some insight into the source of OH. Primary OH, produced from the O_3 photolysis and subsequent reaction of $O(^1D)$ with water vapor (under humid conditions), can only be produced when the GUV222 lamp is on. In contrast, secondary OH, produced from limonene ozonolysis, does not require the lamp to be on. As the ratio $k_{LIM+OH}[OH]$ / $k_{LIM+O3}[O_3]$ is not strongly modulated by the GUV222 lamp, we conclude that most of the OH is secondary, which is consistent with the modeled OH and previous measurements.[16,55,56]

To further evaluate the production of primary OH radicals, chamber experiments exposing hexanal to 222 nm light were performed under humid conditions (Figure S6B). Hexanal reacts efficiently with OH but not with the eluate of O_3. Any removal of hexanal would therefore be due to primary OH formation. Also, photolysis of hexanal is expected to be minimal, and this was confirmed in a chamber experiment exposing hexanal to 222 nm of light under dry conditions (Figure S6A). Figure S6 summarizes the results of these experiments. It was found that removal of hexanal is exceedingly slow under these conditions, indicating that primary OH production is not important for VOC removal in these experiments. In contrast, Barber et al. (2023) found primary OH production to be more important at fluence rates about 18 times larger than the fluence rates in our experiments.[16]

3.2. Formation of Secondary Organic Aerosol. Figure 1 also shows the formation of SOA measured by SMPS resulting from the reactions of limonene induced by the GUV222 lamp. Also included in Figure 1 is the calculated SOA formation from the model. Here, we adjusted the values for the molar yield of gas-phase products of limonene oxidation and used the measured wall deposition rate of particles to obtain a better match with the data. The distribution of SVOC and LVOC for the limonene ozonolysis experiments under dry and humid conditions is shown in Figure S7. The molar yields of the first-generation LVOC and SVOC, and the second-generation LVOC before partitioning, were estimated to be 8.23%, 8.16%, and 95.5%, respectively (assuming a molar mass of 250 g mol^{-1}) to best reproduce the observed SOA formation and growth with the model (see Figure 1 and Formation of Secondary Organic Aerosol for details). The period near the beginning of the experiment saw condensation sink increasing very rapidly (>35 h^{-1} after 1 h; Figure S4).
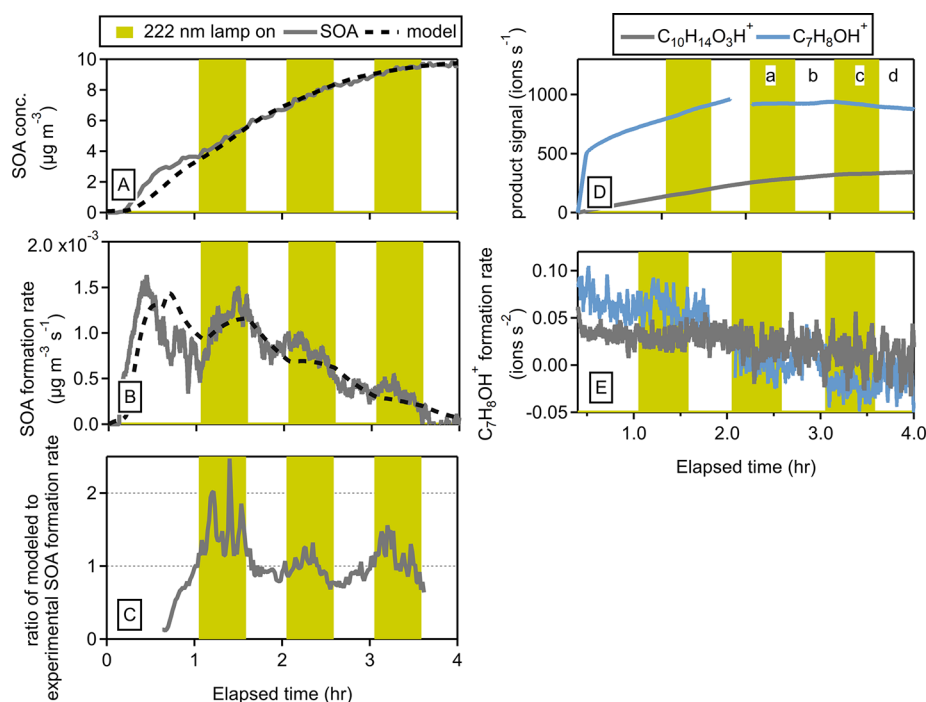
Figure 3. Experimental and modeled SOA produced from the oxidation of limonene (A), the experimental and modeled SOA formation rate (B), and the ratio of the modeled SOA to the experimental SOA formation rates (C) under dry conditions; gas-phase products produced from the oxidation of limonene (D), and the gas-phase products formation rates (E) under dry conditions.

SOA formation is analyzed further in Figure 3. Figure 3B shows the derivative of the SOA concentration versus time, in other words, the SOA formation rate. As the concentrations of both O_3 and OH are modulated by the GUV222 lamp, the SOA formation rate also shows a modulation by the lamp. When the lamp is on, the SOA formation rate increases as the level of O_3 is increased by the lamp. In contrast, when the lamp is off, the SOA formation rate decreases as ozone and limonene are both removed.

Figure 3B also shows the modeled SOA formation rate, which shows a modulation similar to that of the GUV222 lamp. To be clear, the modulation in the model is caused only by the modulation of the O_3 formation by the lamp. The measured and modeled SOA formation rates are in good agreement. To investigate this in more detail, Figure 3C shows the ratio of the modeled SOA formation rate divided by the measured SOA formation rate. Here it is seen that while the ratio hovers around 1 (modeled and measured SOA formation rates agree), there is a slight dependence of this ratio on the lamp: when the lamp is on, the ratio between modeled and measured SOA formation rates increases by ~19% when the lamp is on relative to the periods when the lamp is off. This would suggest that the measured SOA formation rate actually decreases slightly with the GUV222 lamp but the effect is small.

We conclude that the GUV222 lamp causes small but noticeable differences in the SOA formation rate. Nevertheless, the effect is small, and the SOA formation from limonene induced by GUV222 can be described by using well-known ozonolysis reactions. The congruence between modeled SOA formation and experimental results under both dry and humid conditions (shown in Figure 1 and Figure S5), even during GUV222 lamp activation, suggests that the lamp did not substantially impact SOA formation, and the amount of SOA formed is not impacted by the humidity. Next, we will discuss

results from the gas-phase product measurements to study the effects of GUV222 in more detail.

3.3. Formation of Gas-Phase Products. Finally, we studied the effects of the GUV222 lamp on the formation of the gas-phase products. Previous research has identified both the gas-phase products resulting from the ozonolysis of limonene, as well as the underlying reaction mechanisms.[26,27,57−60] Expected products for the ozonolysis of limonene (limonaldehyde, limonaketone, limononic acid, keto-limonaldehyde, and keto-limononic acid) are shown in Figure S8.[26,59] The product mass spectra observed in this work (Figure S8) have some main oxidation products labeled as the expected parent ion (MH[+].) There is significant fragmentation in the Vocus and although there are ways to account for product fragmentation, this was not done here.[61]

To qualitatively evaluate the effect of the 222 nm lamp on the formation of gas-phase products, Figure 3D shows the measured time series for 2 of the ions related to the gas-phase products. After an initial increase in their concentrations, the signals reach a plateau after ~2 h as the formation rates slow down and/or the formation and loss are in steady state. The derivative of the time series, in other words the product formation rates, were calculated (Figure 3E). There are small changes in the time product formation rates for both gas-phase products as the GUV222 light is turned on and off under both humid and dry conditions (for both limonene and α-pinene). The product formation rate for some ions approaches 0, meaning the production and loss of that ion are approaching steady state. The product formation rate for some ions becomes negative, meaning that they are predominantly removed. To summarize this analysis across all *m/z*, we have calculated the changes in product ion signal (Figure 4A) and formation rates (Figure 4B) when the GUV222 lamp is on. Specifically, we calculate the average signal and formation rate during period c (lamp on) and divide it by the average signal
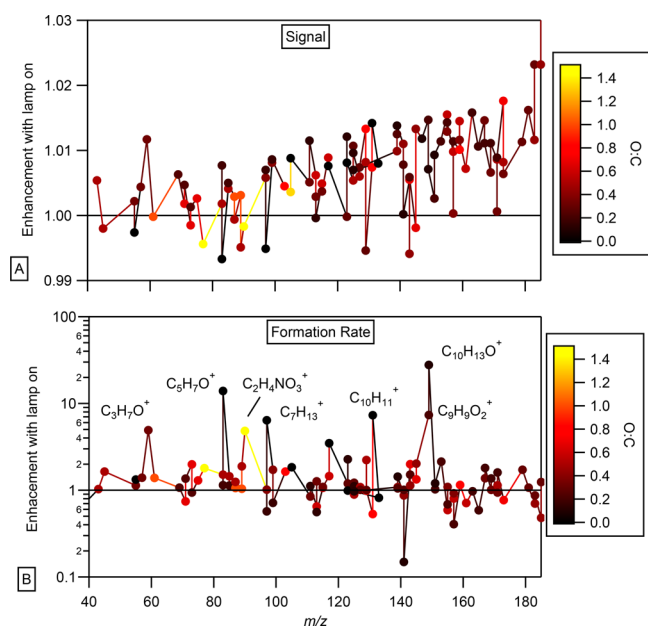
Figure 4. Average signal (A) and the average formation rate (B) of gas-phase products during period c (lamp on) divided by the average formation rates during periods b and d (lamp off) as a function of m/z.

and formation rates during periods b and d (lamp off). The resulting ratios are presented as a function of m/z and colored by oxidation state (O:C) in Figure 4. We included the O/C ratios to look for a possible dependence on functional groups but did not observe an effect. Clearly, the lamp does cause changes in the product formation rates of some gas-phase species (as the values for the above metric range from 1.5×10^{-1} to 2.8×10^{1}), but these do not lead to large changes in the concentration of the gas-phase species in the chamber, as seen in Figure 4A. There appears to be a relationship in the metric indicating that molecules with certain functional groups behave differently; we have not investigated this further. Our goal here was to conduct a qualitative analysis to identify large changes, such as indications of photolysis or any unexpected chemistry linked to the presence of 222 nm light, in the gas-phase products observed during the periods when the lamp was turned on; however, such changes were not detected.

3.4. Implications. While these lamps offer benefits in reducing the spread of airborne illnesses such as COVID-19, it is essential to recognize potential unintended consequences on indoor air quality. The production of ozone by GUV lamps, coupled with the formation of SOA from the reaction of ozone with VOCs such as limonene, underscores the importance of a comprehensive risk assessment. In particular, the health effects associated with ozone exposure, particulate matter, and toxic organic compounds must be carefully evaluated when implementing GUV lamps in indoor environments.

By demonstrating that existing knowledge of limonene ozonolysis adequately describes SOA formation in the presence of GUV222, we provide insights into the potential implications of GUV lamp use on indoor air quality. Importantly, we found that there was no unexpected chemistry and no discernible effect on the expected byproduct formation from limonene oxidation by ozone and OH, so existing chemical models can be used in risk assessment.

However, it is crucial to recognize the complexities of real indoor environments, including the presence of additional ozone sinks, pre-existing particles, and other VOCs, which may influence the efficacy of GUV disinfection and the formation of secondary pollutants. Ultimately, the benefits of disease prevention using GUV must be weighed against the risks associated with the increased ozone, PM2.5 and VOCs indoors produced by GUV lamps. Results such as those reported here can improve our confidence in the models that describe indoor air quality effects. More work is needed to perform such studies in different indoor environments and under different conditions. In addition, more work is needed to quantify the removal of airborne disease vectors by the GUV.

■ ASSOCIATED CONTENT

ⓈＩ Supporting Information

The Supporting Information is available free of charge at https://pubs.acs.org/doi/10.1021/acsestair.4c00065. .

A figure of the emission spectrum of the 222 nm lamp used in chamber experiments (Figure S1); a figure of the of α-pinene ozonolysis experiment summary (Figure S2); a figure of the SOA measurement summary (Figure S3); a figure of the condensation sink (Figure S4); a figure of the modeled and measured experiment summary for the limonene ozonolysis experiment under humid conditions (Figure S5); a figure of the experiment summary for hexanal experiments (Figure S6); a figure of the measured SOA compared to the stacked modeled SOA distribution for limonene dry and humid experiments (Figure S7), a figure of the expected ozonolysis products from limonene and α-pinene highlighted in the product mass spectra (Figure S8); a table of the experimental details (Table S1); a table of relevant reactions used in the kinetic model (Table S2). (PDF)

■ AUTHOR INFORMATION

Corresponding Author

Joost A. de Gouw − *Department of Chemistry, University of Colorado, Boulder, Colorado 80309, United States; Cooperative Institute for Research in Environmental Sciences (CIRES), Boulder, Colorado 80309, United States;* ⓞ orcid.org/0000-0002-0385-1826; Email: Joost.deGouw@colorado.edu

Authors

Olivia J. Jenks − *Department of Chemistry, University of Colorado, Boulder, Colorado 80309, United States; Cooperative Institute for Research in Environmental Sciences (CIRES), Boulder, Colorado 80309, United States;* ⓞ orcid.org/0000-0002-4184-3296

Zhe Peng − *Department of Chemistry, University of Colorado, Boulder, Colorado 80309, United States; Cooperative Institute for Research in Environmental Sciences (CIRES), Boulder, Colorado 80309, United States*

Melinda K. Schueneman − *Department of Chemistry, University of Colorado, Boulder, Colorado 80309, United States; Cooperative Institute for Research in Environmental Sciences (CIRES), Boulder, Colorado 80309, United States;* ⓞ orcid.org/0000-0003-4359-1472

Madison Rutherford − *Department of Chemistry, University of Colorado, Boulder, Colorado 80309, United States;*

Cooperative Institute for Research in Environmental Sciences (CIRES), Boulder, Colorado 80309, United States

Anne V. Handschy − Department of Chemistry, University of Colorado, Boulder, Colorado 80309, United States; Cooperative Institute for Research in Environmental Sciences (CIRES), Boulder, Colorado 80309, United States

Douglas A. Day − Department of Chemistry, University of Colorado, Boulder, Colorado 80309, United States; Cooperative Institute for Research in Environmental Sciences (CIRES), Boulder, Colorado 80309, United States;
  ⓞ orcid.org/0000-0003-3213-4233

Jose L. Jimenez − Department of Chemistry, University of Colorado, Boulder, Colorado 80309, United States; Cooperative Institute for Research in Environmental Sciences (CIRES), Boulder, Colorado 80309, United States;
  ⓞ orcid.org/0000-0001-6203-1847

Complete contact information is available at:
https://pubs.acs.org/10.1021/acsestair.4c00065

Notes

The authors declare no competing financial interest.

■ REFERENCES

(1) Reed, N. G. The History of Ultraviolet Germicidal Irradiation for Air Disinfection. *Public Health Rep.* **2010**, *125* (1), 15−27.

(2) Hart, D. Bactericidal Ultraviolet Radiation in the Operating Room: Twenty-Nine-Year Study for Control of Infections. *J. Am. Med. Assoc.* **1960**, *172*, 1019−1028.

(3) WELLS, W. F.; WELLS, M. W.; WILDER, T. S. The Environmental Control of Epidemic Contagion: I. An Epidemiologic Study of Radiant Disenfection of Air in Day Schools. *Am. J. Epidemiol.* **1942**, *35* (1), 97−121.

(4) McLean, R. The Mechanism of Spread of Asian Influenza. *Am. Rev. Respir. Dis.: General Discussion* **1961**, *83*, 35−40.

(5) Riley, R. L.; Mills, C. C.; Nyka, W.; Weinstock, N.; Storey, P. B.; Sultan, L. U.; Riley, M. C.; Wells, W. F. Aerial Dissemination of Pulmonary Tuberculosis: A Two-Year Study of Contagion in a Tuberculosis Ward. *Am. J. Epidemiol.* **1995**, *142* (1), 3−14.

(6) Jimenez, J. L.; Marr, L. C.; Randall, K.; Ewing, E. T.; Tufekci, Z.; Greenhalgh, T.; Tellier, R.; Tang, J. W.; Li, Y.; Morawska, L.; Mesiano-Crookston, J.; Fisman, D.; Hegarty, O.; Dancer, S. J.; Bluyssen, P. M.; Buonanno, G.; Loomans, M. G. L. C.; Bahnfleth, W. P.; Yao, M.; Sekhar, C.; Wargocki, P.; Melikov, A. K.; Prather, K. A. What Were the Historical Reasons for the Resistance to Recognizing Airborne Transmission during the COVID -19 Pandemic? *Indoor Air* **2022**, *32* (8), No. e13070.

(7) Greenhalgh, T.; Jimenez, J. L.; Prather, K. A.; Tufekci, Z.; Fisman, D.; Schooley, R. Ten Scientific Reasons in Support of Airborne Transmission of SARS-CoV-2. *Lancet* **2021**, *397* (10285), 1603−1605.

(8) Ma, B.; Gundy, P. M.; Gerba, C. P.; Sobsey, M. D.; Linden, K. G. UV Inactivation of SARS-CoV-2 across the UVC Spectrum: KrCl* Excimer, Mercury-Vapor, and Light-Emitting-Diode (LED) Sources. *Appl. Environ. Microbiol.* **2021**, *87* (22), No. e01532-21.

(9) Camargo, C.; Lupien, A.; McIntosh, F.; Menzies, D.; Behr, M. A.; Sagan, S. M. Effectiveness of Germicidal Ultraviolet Light to Inactivate Coronaviruses on Personal Protective Equipment to Reduce Nosocomial Transmission. *Infect. Control Hosp. Epidemiol.* **2022**, *43* (7), 886−891.

(10) Talbot, E. A.; Jensen, P.; Moffat, H. J.; Wells, C. D. Occupational Risk from Ultraviolet Germicidal Irradiation (UVGI) Lamps. *Int. J. Tuberc. Lung Dis.* **2002**, *6* (8), 738−741.

(11) Nardell, E. A.; Bucher, S. J.; Brickner, P. W.; Wang, C.; Vincent, R. L.; Becan-McBride, K.; James, M. A.; Michael, M.; Wright, J. D. Safety of Upper-Room Ultraviolet Germicidal Air Disinfection for Room Occupants: Results from the Tuberculosis Ultraviolet Shelter Study. *Public Health Rep.* **2008**, *123* (1), 52−60.

(12) Buonanno, M.; Ponnaiya, B.; Welch, D.; Stanislauskas, M.; Randers-Pehrson, G.; Smilenov, L.; Lowy, F. D.; Owens, D. M.; Brenner, D. J. Germicidal Efficacy and Mammalian Skin Safety of 222-Nm UV Light. *Radiat. Res.* **2017**, *187* (4), 493−501.

(13) Narita, K.; Asano, K.; Morimoto, Y.; Igarashi, T.; Nakane, A. Chronic Irradiation with 222-Nm UVC Light Induces Neither DNA Damage nor Epidermal Lesions in Mouse Skin, Even at High Doses. *PLoS One* **2018**, *13* (7), No. e0201259.

(14) Kaidzu, S. Re-Evaluation of Rat Corneal Damage by Short-Wavelength UV Revealed Extremely Less Hazardous Property of Far-UV-C. *Photochem. Photobiol.* **2021**, *97*, 505−516.

(15) Peng, Z.; Day, D. A.; Symonds, G. A.; Jenks, O. J.; Stark, H.; Handschy, A. V.; De Gouw, J. A.; Jimenez, J. L. Significant Production of Ozone from Germicidal UV Lights at 222 Nm. *Environ. Sci. Technol. Lett.* **2023**, *10* (8), 668−674.

(16) Barber, V. P.; Goss, M. B.; Franco Deloya, L. J.; LeMar, L. N.; Li, Y.; Helstrom, E.; Canagaratna, M.; Keutsch, F. N.; Kroll, J. H. Indoor Air Quality Implications of Germicidal 222 Nm Light. *Environ. Sci. Technol.* **2023**, *57* (42), 15990−15998.

(17) Link, M. F.; Shore, A.; Hamadani, B. H.; Poppendieck, D. Ozone Generation from a Germicidal Ultraviolet Lamp with Peak Emission at 222 Nm. *Environ. Sci. Technol. Lett.* **2023**, *10* (8), 675−679.

(18) Klepeis, N. E.; Nelson, W. C.; Ott, W. R.; Robinson, J. P.; Tsang, A. M.; Switzer, P.; Behar, J. V.; Hern, S. C.; Engelmann, W. H. The National Human Activity Pattern Survey (NHAPS): A Resource for Assessing Exposure to Environmental Pollutants. *J. Expo. Sci. Environ. Epidemiol.* **2001**, *11* (3), 231−252.

(19) McDonald, B. C.; De Gouw, J. A.; Gilman, J. B.; Jathar, S. H.; Akherati, A.; Cappa, C. D.; Jimenez, J. L.; Lee-Taylor, J.; Hayes, P. L.; McKeen, S. A.; Cui, Y. Y.; Kim, S. W.; Gentner, D. R.; Isaacman-VanWertz, G.; Goldstein, A. H.; Harley, R. A.; Frost, G. J.; Roberts, J. M.; Ryerson, T. B.; Trainer, M. Volatile Chemical Products Emerging as Largest Petrochemical Source of Urban Organic Emissions. *Science* **2018**, *359* (6377), 760−764.

(20) Stönner, C.; Edtbauer, A.; Williams, J. Real-World Volatile Organic Compound Emission Rates from Seated Adults and Children for Use in Indoor Air Studies. *Indoor Air* **2018**, *28* (1), 164−172.

(21) Bernstein, J. A.; Alexis, N.; Bacchus, H.; Bernstein, I. L.; Fritz, P.; Horner, E.; Li, N.; Mason, S.; Nel, A.; Oullette, J.; Reijula, K.; Reponen, T.; Seltzer, J.; Smith, A.; Tarlo, S. M. The Health Effects of Nonindustrial Indoor Air Pollution. *J. Allergy Clin. Immunol.* **2008**, *121* (3), 585−591.

(22) Weschler, C. J. Changes in Indoor Pollutants since the 1950s. *Atmos. Environ.* **2009**, *43* (1), 153−169.

(23) Graeffe, F.; Luo, Y.; Guo, Y.; Ehn, M. Unwanted Indoor Air Quality Effects from Using Ultraviolet C Lamps for Disinfection. *Environ. Sci. Technol. Lett.* **2023**, *10* (2), 172−178.

(24) Logue, J. M.; McKone, T. E.; Sherman, M. H.; Singer, B. C. Hazard Assessment of Chemical Air Contaminants Measured in Residences. *Indoor Air* **2011**, *21* (2), 92−109.

(25) Weschler, C. J.; Shields, H. C.; Naik, D. V. Indoor Ozone Exposures. *JAPCA* **1989**, *39* (12), 1562−1568.

(26) Weschler, C. J.; Shields, H. C. Indoor Ozone/Terpene Reactions as a Source of Indoor Particles. *Atmos. Environ.* **1999**, *33* (15), 2301−2312.

(27) Grosjean, D.; Williams, E. L.; Seinfeld, J. H. Atmospheric Oxidation of Selected Terpenes and Related Carbonyls: Gas-Phase Carbonyl Products. *Environ. Sci. Technol.* **1992**, *26* (8), 1526−1533.

(28) Wainman, T.; Zhang, J.; Weschler, C. J.; Lioy, P. J. Ozone and Limonene in Indoor Air: A Source of Submicron Particle Exposure. *Environ. Health Perspect.* **2000**, *108* (12), 1139–45.

(29) Pagonis, D.; Algrim, L. B.; Price, D. J.; Day, D. A.; Handschy, A. V.; Stark, H.; Miller, S. L.; De Gouw, J. A.; Jimenez, J. L.; Ziemann, P. J. Autoxidation of Limonene Emitted in a University Art Museum. *Environ. Sci. Technol. Lett.* **2019**, *6* (9), 520–524.

(30) Deal, A. M.; Vaida, V. Oxygen Effect on the Ultraviolet-C Photochemistry of Lactic Acid. *J. Phys. Chem. A* **2023**, *127* (13), 2936–2945.

(31) Stockwell, W. R.; Kirchner, F.; Kuhn, M.; Seefeld, S. A New Mechanism for Regional Atmospheric Chemistry Modeling. *J. Geophys. Res. Atmospheres* **1997**, *102* (D22), 25847–25879.

(32) Peng, Z.; Miller, S. L.; Jimenez, J. L. Model Evaluation of Secondary Chemistry Due to Disinfection of Indoor Air with Germicidal Ultraviolet Lamps. *Environ. Sci. Technol. Lett.* **2023**, *10* (1), 6–13.

(33) Duncan, M. A.; Welch, D.; Shuryak, I.; Brenner, D. J. Ocular and Facial Far-UVC Doses from Ceiling-Mounted 222 Nm Far-UVC Fixtures. *Photochem. Photobiol.* **2023**, *99* (1), 160–167.

(34) Nazaroff, W. W.; Weschler, C. J. Indoor Ozone: Concentrations and Influencing Factors. *Indoor Air* **2022**, *32* (1), No. e12942.

(35) Amodio, M.; Dambruoso, P. R.; De Gennaro, G.; De Gennaro, L.; Loiotile, A. D.; Marzocca, A.; Stasi, F.; Trizio, L.; Tutino, M. Indoor Air Quality (IAQ) Assessment in a Multistorey Shopping Mall by High-Spatial-Resolution Monitoring of Volatile Organic Compounds (VOC). *Environ. Sci. Pollut. Res.* **2014**, *21* (23), 13186–13195.

(36) Pytel, K.; Marcinkowska, R.; Zabiegała, B. Investigation on Air Quality of Specific Indoor Environments—Spa Salons Located in Gdynia, Poland. *Environ. Sci. Pollut. Res.* **2021**, *28* (42), 59214–59232.

(37) Liu, X.; Day, D. A.; Krechmer, J. E.; Brown, W.; Peng, Z.; Ziemann, P. J.; Jimenez, J. L. Direct Measurements of Semi-Volatile Organic Compound Dynamics Show near-Unity Mass Accommodation Coefficients for Diverse Aerosols. *Commun. Chem.* **2019**, *2* (1), 98.

(38) Day, D. A.; Fry, J. L.; Kang, H. G.; Krechmer, J. E.; Ayres, B. R.; Keehan, N. I.; Thompson, S. L.; Hu, W.; Campuzano-Jost, P.; Schroder, J. C.; Stark, H.; DeVault, M. P.; Ziemann, P. J.; Zarzana, K. J.; Wild, R. J.; Dubè, W. P.; Brown, S. S.; Jimenez, J. L. Secondary Organic Aerosol Mass Yields from NO$_3$ Oxidation of α-Pinene and Δ-Carene: Effect of RO$_2$ Radical Fate. *J. Phys. Chem. A* **2022**, *126* (40), 7309–7330.

(39) Krechmer, J. E.; Day, D. A.; Ziemann, P. J.; Jimenez, J. L. Direct Measurements of Gas/Particle Partitioning and Mass Accommodation Coefficients in Environmental Chambers. *Environ. Sci. Technol.* **2017**, *51* (20), 11867–11875.

(40) DeCarlo, P. F.; Kimmel, J. R.; Trimborn, A.; Northway, M. J.; Jayne, J. T.; Aiken, A. C.; Gonin, M.; Fuhrer, K.; Horvath, T.; Docherty, K. S.; Worsnop, D. R.; Jimenez, J. L. Field-Deployable, High-Resolution, Time-of-Flight Aerosol Mass Spectrometer. *Anal. Chem.* **2006**, *78* (24), 8281–8289.

(41) Kimmel, J. R.; Farmer, D. K.; Cubison, M. J.; Sueper, D.; Tanner, C.; Nemitz, E.; Worsnop, D. R.; Gonin, M.; Jimenez, J. L. Real-Time Aerosol Mass Spectrometry with Millisecond Resolution. *Int. J. Mass Spectrom.* **2011**, *303* (1), 15–26.

(42) Nault, B. A.; Campuzano-Jost, P.; Day, D. A.; Schroder, J. C.; Anderson, B.; Beyersdorf, A. J.; Blake, D. R.; Brune, W. H.; Choi, Y.; Corr, C. A.; De Gouw, J. A.; Dibb, J.; DiGangi, J. P.; Diskin, G. S.; Fried, A.; Huey, L. G.; Kim, M. J.; Knote, C. J.; Lamb, K. D.; Lee, T.; Park, T.; Pusede, S. E.; Scheuer, E.; Thornhill, K. L.; Woo, J.-H.; Jimenez, J. L. Secondary Organic Aerosol Production from Local Emissions Dominates the Organic Aerosol Budget over Seoul, South Korea, during KORUS-AQ. *Atmospheric Chem. Phys.* **2018**, *18* (24), 17769–17800.

(43) Sueper, D. 2021. https://cires1.colorado.edu/jimenez-group/ToFAMSResources/ToFSoftware/. Accessed May 23, 2023.

(44) Day, D. A.; Cubison, M. J.; Palm, B. B.; Jimenez, J. L. Scanning Mobility Particle Sizer Loader and Plotter, 2024. https://gitlab.com/JimenezGroup/smps_loader_plotter (accessed 2024-02-19).

(45) Kuwata, M.; Zorn, S. R.; Martin, S. T. Using Elemental Ratios to Predict the Density of Organic Material Composed of Carbon, Hydrogen, and Oxygen. *Environ. Sci. Technol.* **2012**, *46* (2), 787–794.

(46) Canagaratna, M. R.; Jimenez, J. L.; Kroll, J. H.; Chen, Q.; Kessler, S. H.; Massoli, P.; Hildebrandt Ruiz, L.; Fortner, E.; Williams, L. R.; Wilson, K. R.; Surratt, J. D.; Donahue, N. M.; Jayne, J. T.; Worsnop, D. R. Elemental Ratio Measurements of Organic Compounds Using Aerosol Mass Spectrometry: Characterization, Improved Calibration, and Implications. *Atmospheric Chem. Phys.* **2015**, *15* (1), 253–272.

(47) Xu, W.; Lambe, A.; Silva, P.; Hu, W.; Onasch, T.; Williams, L.; Croteau, P.; Zhang, X.; Renbaum-Wolff, L.; Fortner, E.; Jimenez, J. L.; Jayne, J.; Worsnop, D.; Canagaratna, M. Laboratory Evaluation of Species-Dependent Relative Ionization Efficiencies in the Aerodyne Aerosol Mass Spectrometer. *Aerosol Sci. Technol.* **2018**, *52* (6), 626–641.

(48) Nault, B. A.; Croteau, P.; Jayne, J.; Williams, A.; Williams, L.; Worsnop, D.; Katz, E. F.; DeCarlo, P. F.; Canagaratna, M. Laboratory Evaluation of Organic Aerosol Relative Ionization Efficiencies in the Aerodyne Aerosol Mass Spectrometer and Aerosol Chemical Speciation Monitor. *Aerosol Sci. Technol.* **2023**, *57* (10), 981–997.

(49) Kulmala, M.; Maso, M. D.; Makela, J. M.; Pirjola, L.; Vakeva, M.; Aalto, P.; Miikkulainen, P.; Hameri, K.; O'Dowd, C. D. On the Formation, Growth and Composition of Nucleation Mode Particles. *Tellus B* **2001**, *53* (4), 479–490.

(50) Peng, Z.; Jimenez, J. L. KinSim: A Research-Grade, User-Friendly, Visual Kinetics Simulator for Chemical-Kinetics and Environmental-Chemistry Teaching. *J. Chem. Educ.* **2019**, *96* (4), 806–811.

(51) Peng, Z.; Jimenez, J. L. Radical Chemistry in Oxidation Flow Reactors for Atmospheric Chemistry Research. *Chem. Soc. Rev.* **2020**, *49* (9), 2570–2616.

(52) Krechmer, J. E.; Day, D. A.; Jimenez, J. L. Always Lost but Never Forgotten: Gas-Phase Wall Losses Are Important in All Teflon Environmental Chambers. *Environ. Sci. Technol.* **2020**, *54* (20), 12890–12897.

(53) Atkinson, R. Kinetics and Mechanisms of the Gas-Phase Reactions of the Hydroxyl Radical with Organic Compounds under Atmospheric Conditions. *Chem. Rev.* **1986**, *86* (1), 69–201.

(54) Shu, Y.; Atkinson, R. Rate Constants for the Gas-Phase Reactions of O$_3$ with a Series of Terpenes and OH Radical Formation from the O$_3$ Reactions with Sesquiterpenes at 296 ± 2 K: GAS-PHASE REACTIONS OF O$_3$. *Int. J. Chem. Kinet.* **1994**, *26* (12), 1193–1205.

(55) Atkinson, R.; Aschmann, S. M. Hydroxyl Radical Production from the Gas-Phase Reactions of Ozone with a Series of Alkenes under Atmospheric Conditions. *Environ. Sci. Technol.* **1993**, *27* (7), 1357–1363.

(56) Aschmann, S. M.; Arey, J.; Atkinson, R. OH Radical Formation from the Gas-Phase Reactions of O3 with a Series of Terpenes. *Atmos. Environ.* **2002**, *36* (27), 4347–4355.

(57) Grosjean, D.; Williams, E. L.; Grosjean, E.; Andino, J. M.; Seinfeld, J. H. Atmospheric Oxidation of Biogenic Hydrocarbons: Reaction of Ozone with. Beta.-Pinene, D-Limonene and Trans-Caryophyllene. *Environ. Sci. Technol.* **1993**, *27* (13), 2754–2758.

(58) Ham, J. E.; Harrison, J. C.; Jackson, S. R.; Wells, J. R. Limonene Ozonolysis in the Presence of Nitric Oxide: Gas-Phase Reaction Products and Yields. *Atmos. Environ.* **2016**, *132*, 300–308.

(59) Wang, L.; Wang, L. The Oxidation Mechanism of Gas-Phase Ozonolysis of Limonene in the Atmosphere. *Phys. Chem. Chem. Phys.* **2021**, *23* (15), 9294–9303.

(60) Chen, W.; Ye, Y.; Hu, W.; Zhou, H.; Pan, T.; Wang, Y.; Song, W.; Song, Q.; Ye, C.; Wang, C.; Wang, B.; Huang, S.; Yuan, B.; Zhu, M.; Lian, X.; Zhang, G.; Bi, X.; Jiang, F.; Liu, J.; Canonaco, F.; Prevot, A. S. H.; Shao, M.; Wang, X. Real-Time Characterization of Aerosol Compositions, Sources, and Aging Processes in Guangzhou During

PRIDE-GBA 2018 Campaign. *J. Geophys. Res. Atmospheres* **2021**, *126* (16), No. e2021JD035114.

(61) Jenks, O. J.; DeVault, M. P.; Ziola, A. C.; Morris, M. A.; Schueneman, M. K.; Stark, H.; Jimenez, J. L.; Ziemann, P. J.; De Gouw, J. A. Investigation of Gas-Phase Products from the NO_3 Radical Oxidation of Δ-3-Carene. *ACS Earth Space Chem.* **2023**, *7* (5), 1097−1106.